❒   168

Investigation of deformations of ballasted railway track during collapse using the Digital Image Correlation Method (DICM)

Szabolcs Szalai[1], Balázs Eller[1], Erika Juhász[1], Majid Rad Movahedi[1], Attila Németh[1], Dániel Harrach[1], Gusztáv Baranyai[1], Szabolcs Fischer[1]

[1] Szechenyi Istvan University, Gyor, Hungary, e-mail: szalaisz@sze.hu, e-mail: eller.balazs@sze.hu, e-mail: juhasz.erika@sze.hu , e-mail: majidmr@sze.hu, e-mail: nemeth.attila@sze.hu, e-mail: harrach.daniel@sze.hu, e-mail: baranyai.gusztav@hallgato.sze.hu, e-mail: fischersz@sze.hu

Article Info	ABSTRACT
	This paper summarizes the results of laboratory tests in which the authors investigated the effects of extremely high vertical load to a railway track segment. The segment consisted of a cut concrete sleeper (contact area: 290×390 mm) with a pair of direct-elastic rail fasteners; the sleeper pieces had a standard, full height; the structure had a typical 350 mm depth railway ballast, underneath approx. 200 mm sandy gravel supplementary layer. The whole assembly was built in a 2.00×2.20 m area wooden rack. The deformations due to the approx. 150 kN static concentrated vertical force were measured and recorded by Digital Image Correlation Method (DICM), ensuring the GOM ATOS technology. The 150 kN peak load meant 1326 kPa vertical stress at the sleeper-ballast interface. The 3D geometry was scanned before the loading and after the collapse. In this way, the comparison was able to be executed. The maximum vertical deformation was 115 mm. The DICM technique is a relatively new methodology in civil engineering; however, it has been applied for more than ten years in mechanical engineering. Therefore, the authors investigated the applicability of DICM in this field. As a result, the pre and the post-states were determined in 3D. The displacement of the ballast particles was able to be defined with the possibility of drawing the displacement trajectories of given points. The DICM can be a valuable methodology in railway engineering, e.g., laboratory tests and field test applications.

Corresponding Author:

Szabolcs Fischer,
Szechenyi Istvan University.
Email: fischersz@sze.hu

1. Introduction

Most of the railway tracks constructed all over the world have ballasted (super)structures, which can be said to be a well-proven traditional railway track (Rampat, 2018; Grossoni et al., 2021; Gouchong & Haiyan, 2021; Fischer, 2021; Eller et al., 2022; Przybyłowicz et al., 2022; Kurhan & Fischer, 2022; Fischer, 2022; Jóvér et al., 2022).

Railway superstructures need to resist a relatively high load due to the vehicles (passenger and freight trains) running on them. Therefore, it is necessary to calculate for each axle passing through the load of the vehicles, which usually means a maximum static load of 225 kN on the rails for standard gauge (i.e., 1435 mm). These loads should be interpreted as separate static and dynamic loads (Kurhan & Kurhan, 2019). The direct force transmitted to the rails is distributed to the sleepers and rail fastening systems, as well as to the ballast bed

(superstructure) below them, and then to the protective layers (in other words: supplementary layers) and substructure.

The ballast layer consolidation was investigated by several researchers using different methods (Sysyn et al., 2018; Sysyn et al., 2019; Juhász & Fischer, 2021). These methods are related to laboratory tests, field tests, numerical modeling, finite element, as well as discrete element modeling, etc. In addition, it has to be mentioned, the track's vertical deformation (settlement) is influenced by many other parameters of the railway permanent way (Kurhan & Havrylov, 2020; Kurhan & Leibuk, 2020; Habashneh, 2021; Ahmad, 2021). If someone wants to calculate and/or model the whole deformation, most of the parameters and effects have to be taken into account.

Part of our research to date has examined ballast (crushed stone) fragmentation using various visual imaging devices 3D scanner, in which the ballast bed itself was loaded mainly into closed vessels or boxes of various sizes (e.g., shear box or closed-ended, capped HDPE tube). In the authors' previous publications, they have already measured deformations and changes with the GOM system, focusing on the fragmentation of smaller aggregates (Juhász & Fischer, 2019a; Juhász & Fischer, 2020).

However, load tests (static and dynamic) in closed boxes do not resemble real ballast bed conditions, so a new experiment methodology has been developed and applied. The prototype was built to see the possible results and the incidental weaknesses of the measurement to improve our experimental possibilities.

In the present paper, a new method is introduced and detailed: digital image correlation method (DIC method or DICM) (Szalai, 2021; Szalai & Dogossy, 2021) for measuring a real ballasted railway permanent way in the laboratory. The DICM is relatively new in civil engineering; however, the mechanical engineering applications are also well-known. An extremely high static vertical load was applied to a sleeper piece, and the 3D deformation was recorded by GOM ATOS and GOM TRITOP, which was concluded a so-called collapse effect related to the ballasted track.

2. Materials and methods

2.1 3D optical photogrammetry and 3D optical coordinate measurement systems

A large sample was measured during the research, which meant several difficulties. The deformation measurement is not possible with the GOM ARAMIS system/methodology presented in the authors' previous article (Szalai et al., 2022), so the GOM TRITOP system was applied. The reason for their usage is twofold, in addition to deformation measurement, 3D surface digitization of large objects is used to accelerate the measurement and reduce errors so that the reference points can be pre-measured with adequate accuracy.

GOM TRITOP

The GOM TRITOP measuring system is a flexible and easy-to-carry optical photogrammetry system (see Fig. 1), practically an optical 3D coordinate measuring machine (CMM). It works on the principle of photogrammetry as opposed to the usual tactile measuring equipment. The system consists of a high-resolution digital single-lens reflex (DSLR) camera, high-quality measurement lenses, coded reference points, and so-called calibration bars. Like traditional measuring machines, the system records the spatial position of the coordinates of discrete points, which can be applied for several purposes. Two main applications of the system have also been used in the present research and related article: deformation measurement and reference point field measurement for GOM ATOS systems. In addition, its main areas of application are the measurement of sheet metal parts and bodies, the quality control of large objects, the inspection of assembled elements, and the verification of parts.

The great advantage of the GOM TRITOP system is that thanks to its mobile set-up and structure, it can accurately determine the 3D coordinates of each point (reference point) of the object to be measured between different measurement states and calculate the displacement of the specimen. However, it is essential to mention that a quasi-static state is required during the measurement (R-Design Studio, 2022).

Figure 1. GOM TRITOP measuring methodology

Principle of measurement

The measurement aims to determine the reference points' coordinates, which are pre-glued to the object's surface to be measured. Moreover, the reference points' spatial position and spatial relationship are known with its help, so the position of the sensor in space will be determined during the subsequent GOM ATOS measurement, as it already "knows" the reference points.

The principle of measurement is the so-called photogrammetry, which is based on the principle of triangulation, which is a measurement methodology for determining spatial coordinates, for which photographs provide the necessary basic information.

Uncoded reference points and coded reference points are needed to perform effective measurement. The system uses these coded points to orient photographs taken at different positions during photogrammetry. Coded points can be distinguished based on their unique position and specific patterns; the system uses them to determine the position of non-coded points in space. In addition, it is necessary to apply so-called measuring bars (scale bars) to determine the exact size of the object. The application of this methodology can ensure the high measurement accuracy of large objects and make complex-shaped pieces easy to measure.

The GOM TRITOP system typically uses black and white images for measurements. During it, the number of pixels (pixel resolution) of the images is not necessarily decisive, but the optical resolution of the objective or lens is more important. The system examines the grayscale gradient (transition) between pixels. It applies coded reference points for "joining" the taken images, so it is essential that images taken at different positions always have at least three common coded reference points with the previous image. In addition, the recognition and identification of uncoded points is a critical task, for which the GOM uses a special "ellipse searching" algorithm. For both types of points, the black and white color combination is very important. When searching for an ellipse, the measurement target is displayed as an ellipse when viewed at a given angle. The definition of the starting point is approximately at the center of the ellipse. The system then radially examines where the grayscale transition occurs, thus determining the outline of the circles or ellipses. (Funke, 2016; Buń et al., 2015; Koutecký et al., 2013)

GOM ATOS

A GOM ATOS TripleScan high-precision industrial optical 3D scanner was applied for the research (see Fig. 2). The GOM ATOS systems are widely used in a variety of industries, with a wide range of measurement possibilities, e.g., from measurements of a complete aircraft to small electronic components. Measuring the entire surface of the part, the device (instrument) captures a dense point cloud or polygon mesh that accurately describes the geometric shape of the object, showing invisible defects, thus making production faster and more efficient. On the measured surface, the measuring instrument projects a stripe pattern based on a precise Gray-code, which is recorded by two cameras simultaneously (DIC) in accordance with the stereo camera principle. Because both of the cameras and the projector are calibrated, the 3D surface points can be triangulated from any two viewpoints in the three different units. The projector uses low-frequency blue light to help eliminate interfering ambient light effects. The resolution of the system is 0.01 mm; the measurement accuracy depends on the measurement range. The cameras are 5, 8, 12 megapixel (MP), and industrial measurement lenses. The measuring distance can be varied between 0.49 and 2.0 m. The size of the area that can be scanned at one time can be changed from 38×29 mm to 2000×1500 mm, also according to the measuring range. In general, micron (0.001 mm) accuracy can be achieved for small products, and a few tenths accuracy for large pieces (Szalai et al., 2022).

Figure 2. GOM ATOS measuring methodology

Principle of measurement

The measurement technology of GOM ATOS 3D scanners based on the principle of triangulation. The projector unit projects a stripe pattern (based on Gray-code) of different widths and light intensities on the object to be measured, in which case the charge-coupled device (CCD) detects a change in the phase-shifting sinusoidal light intensity reflected from the object. These patterns are recorded by two cameras. According to the heterodyne light interference principle, the instrument applies multiple phase shifts for maximum "subpixel" accuracy. Based on the transformation equations of optical imaging, the computer automatically calculates the 3D coordinates of each camera pixel with high accuracy in some seconds. In order to digitize an object over the entire surface, several independent measurements from different views are required. The GOM ATOS system uses a special reference point recognition technique to automatically merge data from different views. At the same time as measuring the object, the system automatically identifies the reference points that must be placed on the object, the surrounding geometry or the mounting before the measurement. Using the reference points, all measurement results are combined in a common global coordinate system. When measuring large objects, if the measuring range is no longer large enough for the size of the object to be measured, the concatenation error may increase, so the GOM ATOS measurement can be combined with the GOM TRITOP measurement to increase the accuracy. This methodology was also applied in the present research. After scanning, the software calculates a high-resolution dynamic polygon grid that presents on(to) the object's surface.

It is important to note that both the GOM TRITOP and GOM ATOS measuring systems are calibrated using a photogrammetric method, during which the temperature, geometric configuration, and lens distortion parameters are reconciled. (GOM, 2022; GOM GmbH, 2011; Goda et al., 2019)

2.2 Presentation of new type railway tests from a 3D measurement perspective

A 2.00×2.20 m frame of OSB sheets (as a wooden rack) was formed in the laboratory under a dynamic actuator, in which a protective layer of sandy gravel was compacted every 5-8 centimeters, and then a compacted ballasted superstructure was formed simulating a 'bedding', as shown in Fig. 3. However, the bearing capacity was only 16.33 MPa; this result did not influence the main direction of this measurement. Furthermore, under the protective layer, 1.20×1.20 m underlay rubber duvet (boards) were used to decrease the rigidity of the concrete supporting structure.
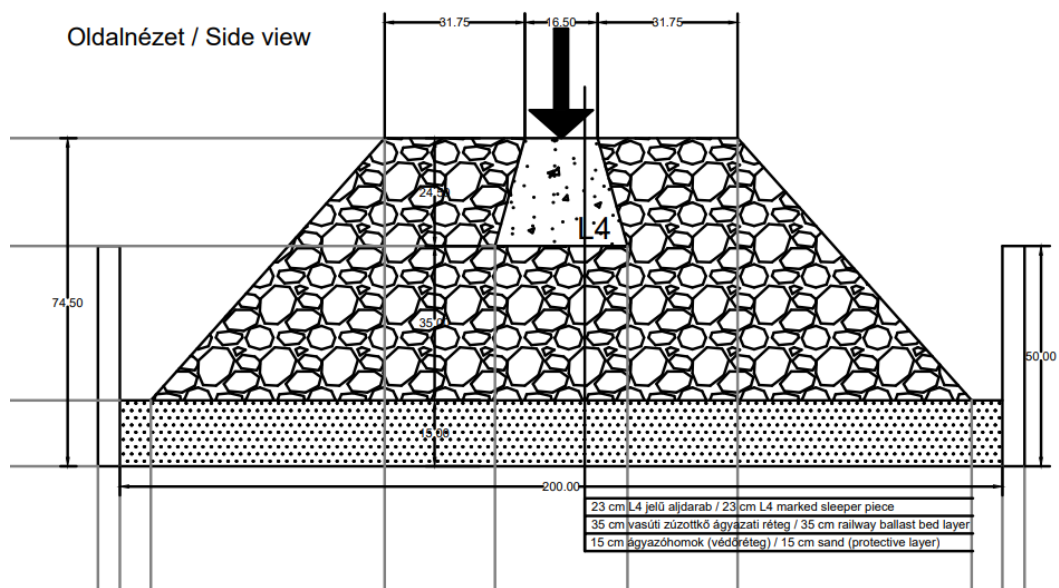
Figure 3. First design (conceptional) drawing of the laboratory test in AutoCAD software

Figure 4. The test set-up: compacted sandy gravel layer on under ballast mat (left side); the constructed ballast bed part (right side)

Approximately a quarter of "L4" marked/type (MABA Hungaria Ltd., 2017) concrete sleeper piece has been embedded in the upper layer of the ballast bed, for which the pair of direct-elastic rail fastening systems (Vossloh, elastic type clamps) have already been assembled and applied. The contact area of the lower plane with the crushed stone is 290×390 mm.

Inside the ballast bed, several stones were hidden, painted in different colors (green, yellow, orange, pink, and blue), and their position was recorded. The stones were scanned by GOM ATOS in 3D.

The railway ballast material was transported from the quarry of Szob (Colas Északkő Ltd., Hungary). Quarry of Szob carried out the obligatory tests related to the crushed stone production process (e.g., particle size distribution). The provided set of crushed stone is suitable for railway use.

Figure 5. The 'hidden' and scanned colored elements in the ballast

Parameters:
- the height of the sleeper: 23 cm (MABA Hungaria Ltd. type sleeper, L4 marked),
- the bottom contact area of the sleeper: 29×39 cm,
- the thickness of the ballast bed: approx. 35 cm (31.5/50, B type ballast bed according to EN 13450:2002 (CEN, 2002)),
- the compaction of the railway ballast material was executed in 4 series/phases on each 10 cm height (see Fischer, 2016),
- the thickness of the sandy gravel supplementary layer: approx. 15 cm (the particle size distribution is shown in Fig. 6 and Table 1, it can be seen that in the interval between 0.063 and 0.25 mm, the measured values don't fully meet with the lower limit line, with some percentages the sample contained less finer content than the required. It has to be mentioned that the authors' aim was not strictly the fact using a granular supplementary layer entirely fitting to the requirement, only the possibility to simulate and model an elastic layer under the track),
- $E_{2,stat,supplementary\ layer}$=16.33 MPa according to MSZ 2509-3:1989 (Hungarian Standards, 1989) (see Fig. 7),
- size of the wooden rack: 2.00 x 2.20 m width, approx. 25 cm height,
- the thickness of the rubber under ballast mat (UBM) layer (here, it was under the supplementary sandy gravel layer): 3 cm,
- the static force (peak load) applied: approx. 150 kN,
- the dynamic force applied: sinusoidal between 5 and 71 kN (according to Fischer (2017), however, in the recent test, there was not any dynamic/fatigue load, only static).
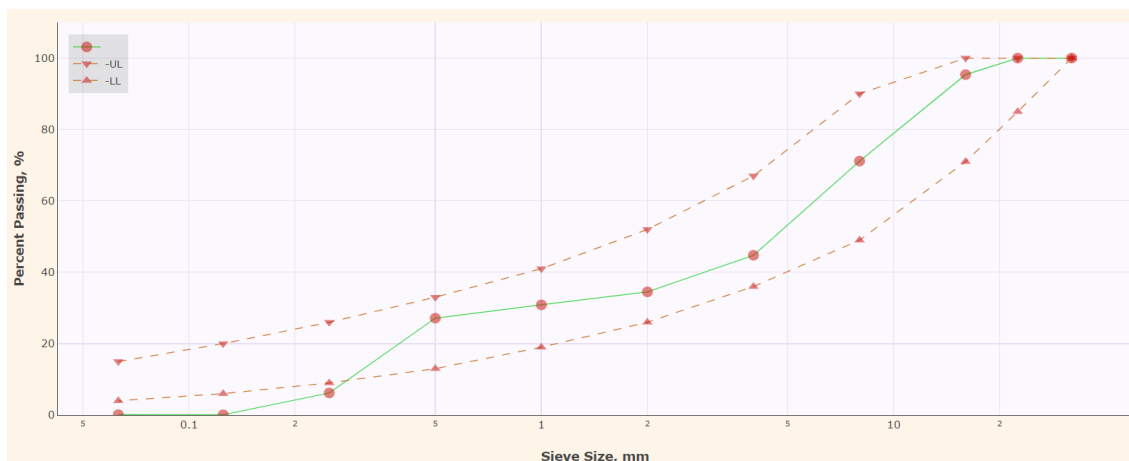
Figure 6. Particle size distribution of sandy gravel supplementary layer (visualization with the help of Transcalc (2022)) according to D.11 [Hungarian State Railways, 2020]

Table 1. Particle size distribution of sandy gravel supplementary layer

Siece size [mm]	Weight retained [g]	Cumulated weight retained [g]	Percentage passing [%]
32	0	0	100
16	260.07	260.07	95.37
8	1362.02	1622.09	71.14
4	1481.84	3103.93	44.77
2	577.03	3680.96	34.51
1	204.24	3885.20	30.87
0.5	209.73	4094.93	27.14
0.25	1177.37	5273.0	6.19
0.125	344.06	5616.36	0.07
0.063	0.87	5617.23	0.11
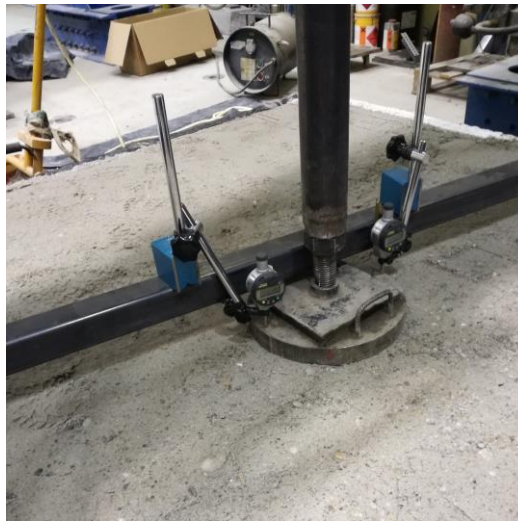
Figure 7. Static load plate test

The superstructure was recorded visually in the unloaded and the loaded state (both before and after the loading) with photos (regular photographs and GOM TRITOP) and also a professional 3D scanner (GOM ATOS). The applied peak load, in its proportions, meant a much higher load on the ballast bed than the load value in reality, so this examination illustrates huge total obsolescence. The 150 kN vertical peak load meant 1326 kPa vertical stress at the sleeper-ballast interface, representing 6.7 times the axle load of 225 kN allowed in the European Union and Hungary.

The essence of the study is to examine the different parameters (fragmentation, compaction, displacement) of the ballast bed statically and then dynamically loaded through the sleeper. Aware of the results, we are confident that a procedure can be developed to determine the degree of fragmentation of the ballast bed, which could help predict the replacement of the ballast, e.g., by discovering a factor/parameter/number of the cycle (year). A (precisely adjusted) "impact" by an actuator would be considered equivalent to passing an axis during dynamic fatigue.

This is aided by measurements with a 3D scanner (GOM ATOS) and photogrammetry method (GOM TRITOP), which is able to examine the displacements of the elements of the aggregate and the sleeper with approx. 0.01-millimeter accuracy (see Chapters 2.1 and 3).

2.3. Validation processes

The validation process of the measuring systems related to deformation measurements can be read in Szalai et al. (2022). The accuracy of the measuring systems was also determined.

3. Measurement setup and sample preparation processes

The measurement task was divided into two parts. Examination of the deformation of the modeled railway permanent way segment and the full 3D surface digitization and geometric measurement of the different states.

The application of the GOM TRITOP measurement methodology, as described in Chapter 2.1, is twofold; with the help of the system, it is possible to measure the deformation between different states (by measuring the displacement of reference points) and to accelerate the GOM ATOS measurement and increase the measurement accuracy.

The authors applied the GOM TRITOP Nikon D7100 camera with Schneider fixed optics, 1.0 m measuring rods, and associated 5 mm coded reference points for the study. To prepare for the experiment, 5 mm unencoded reference points were applied to the stones at approximately 200 mm distances on the surface of the stones. To make the measurement easier, 24-page 3D printed measurement "bodies" were placed (they can be named as "eikosi-tessera-eders"), see Figs. 8-9. In the first phase of the measurement, the calibration photos were taken according to the GOM specification, and then 80-90 images were taken of each phase. The evaluation was performed in the GOM ATOS 2018 software.

The MV560 measuring range and the associated Schneider optics, as well as Titinar projection unit were applied for the GOM ATOS method (Fig. 8). A measuring distance of 800 mm is optimal for the measuring range, so the product to be measured must be placed at this distance. Close to the full 360° surface digitization, the sample was measured by walking around this distance. Before starting the measurement, the system must be calibrated with the calibration plate belonging to the measuring range. Reference points are required to concatenate images taken in each position. These 5 mm reference points were read from the GOM TRITOP measurement. The surface of the crushed stones showed no reflection, so no further preparatory operation was required. At the end of the measurement, the surface was described with nearly 25 million measurement points for each condition (i.e., state).
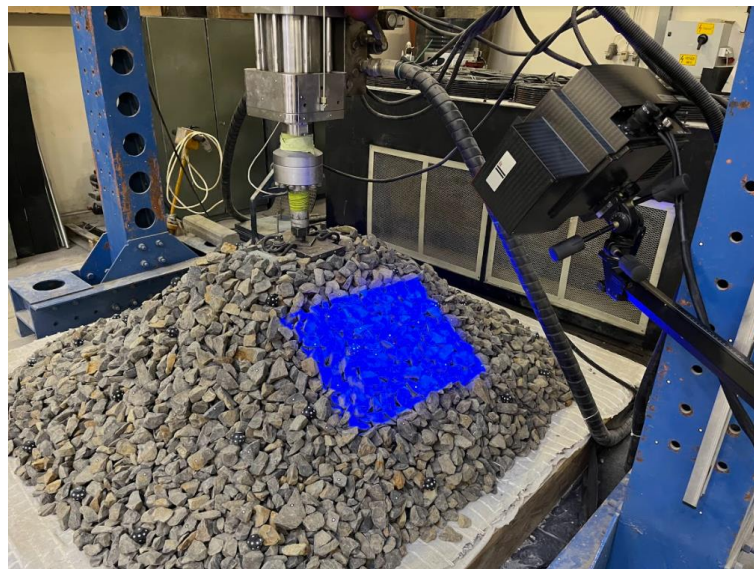
Figure 8. Set-up for GOM TRITOP and GOM ATOS measurement

Figure 9. The 3D printed plastic body (i.e., "eikosi-tessera-eder") with point stickers

4. Results and discussion

Unfortunately, the loading diagram can't be exported from the TestBuilder software of the applied BiSS actuator due to an instantaneous data recording fault or error. The authors were able to register only the peak (last) data pair. It is the reason why no loading diagram has been published in this article. (Because of the fact that the authors' aim was not to assess at this stage the load-bearing capacity of the test assemblage in the laboratory, but the possibility of the application of DICM in civil engineering and/or railway engineering, it was enough for the investigation.)

The design of the laboratory underwent a spectacular change. The middle part of the cross-section at the rest phase has undergone considerable compaction due to the probably improperly compacted sandy gravel and ballasted bed. The test design before and after loading is shown in Figs. 10-11.

Figure 10. Photos of the laboratory sample before (left-hand side) and after loading (right-hand side)

It is clear that the height of the ballast bed has been significantly reduced in the middle (loaded) part.

Figure 11. Photos of the sleeper piece before (left-hand side) and after loading (right-hand side)

It can be clearly seen that the railway sleeper piece has turned a bit slightly and pressed under the top layer of crushed stone.

According to the measurement results, the value of the maximum subsidence exceeded 115 millimeters.

Significant deformation was observed in the area under the reinforced concrete sleeper piece pressed by the actuator. Based on the results from the 3D scanner, the cross-sectional design also shows that the greatest displacement occurred at these locations. In addition to the greatest deformation, significant deformation was seen on the outer parts and further away from the pressure point.
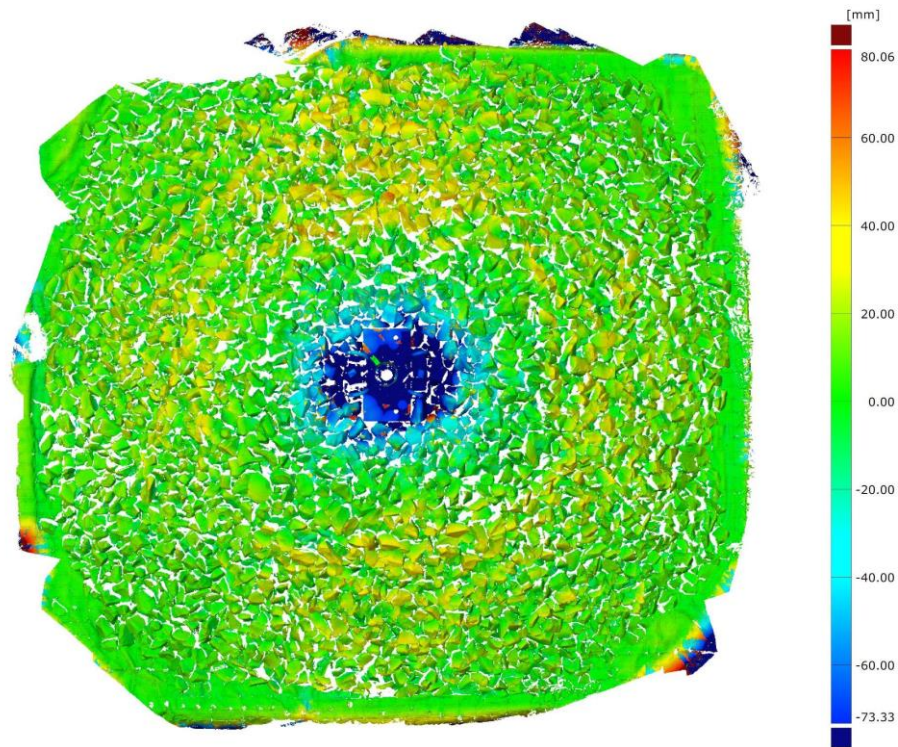
Figure 12. Displacement of the test sample in 3D, top view – GOM ATOS
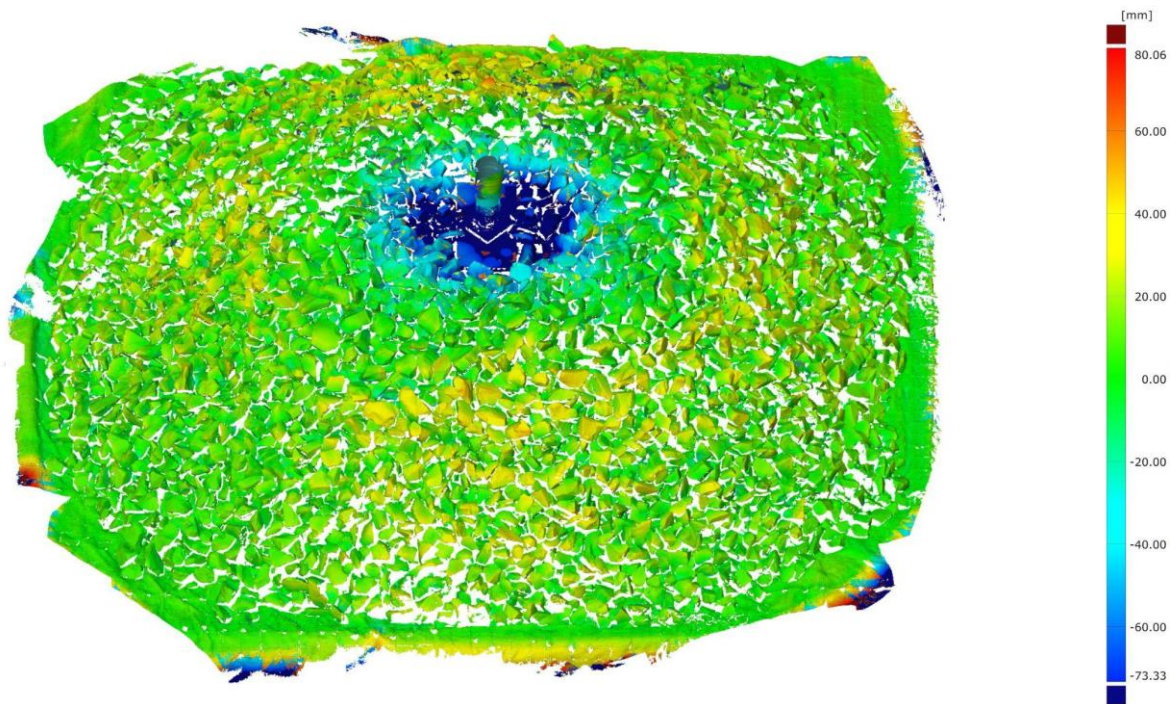
Figure 13. Displacement of the test sample in 3D, axonometric view – GOM ATOS #1
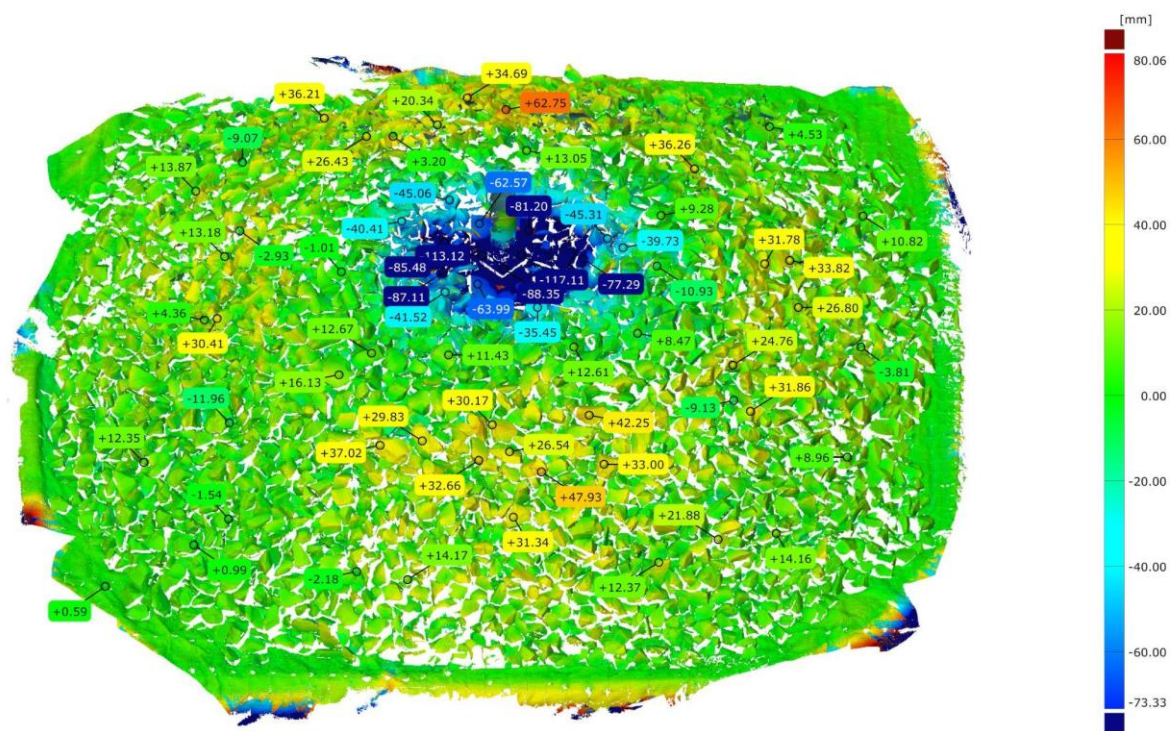
Figure 14. Displacement of the test sample in 3D with flags, axonometric view – GOM ATOS
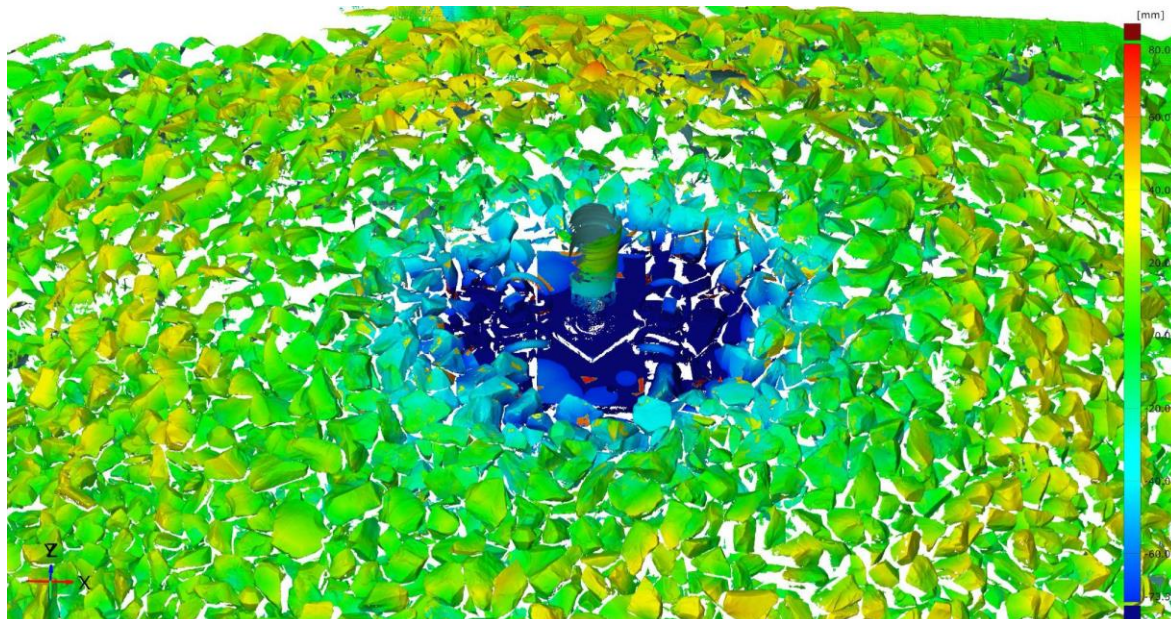
Figure 15. Displacement of the critical part of the test sample in 3D, axonometric view – GOM ATOS
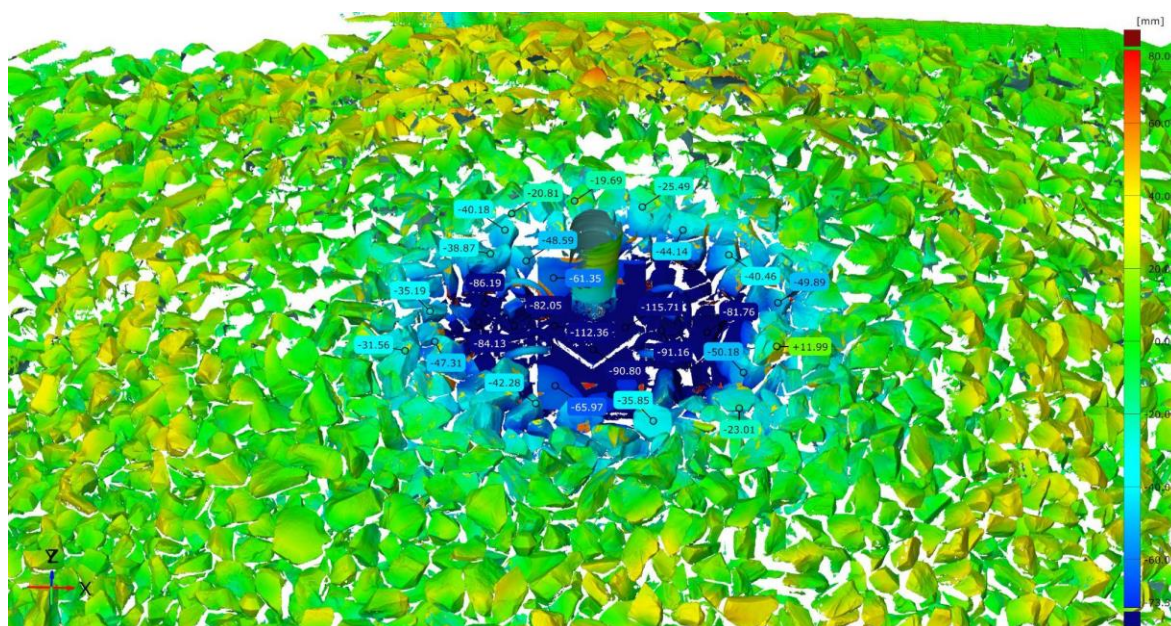
Figure 16. Displacement of the critical part of the test sample in 3D with flags, axonometric view – GOM ATOS
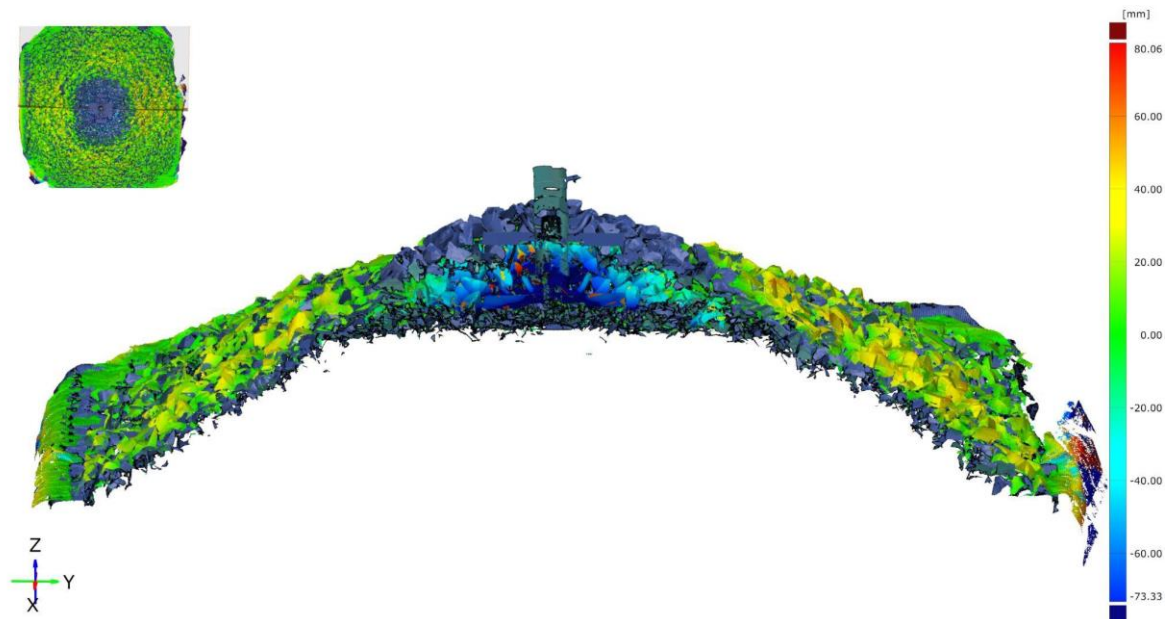
Figure 17. Displacement of the test sample in 3D, combined cross-section and axonometric view –
GOM ATOS #1
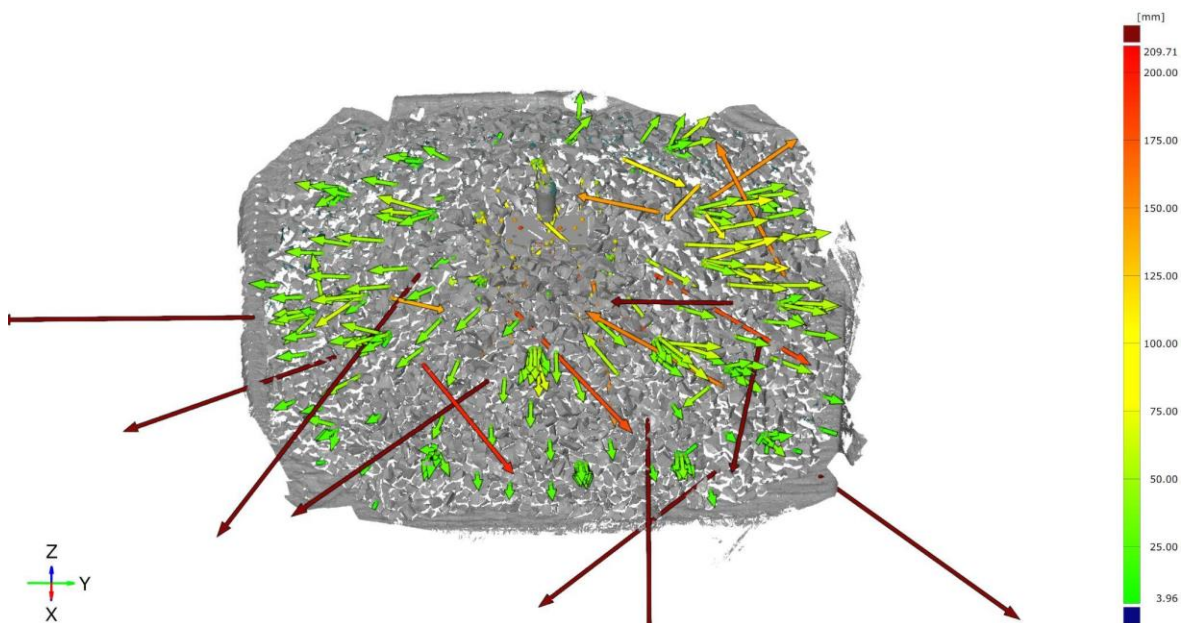
Figure 18. Displacement of the test sample in 3D, axonometric view – GOM TRITOP #2 (the
long brown and red arrows can be neglected, they are related to the enconded reference points)
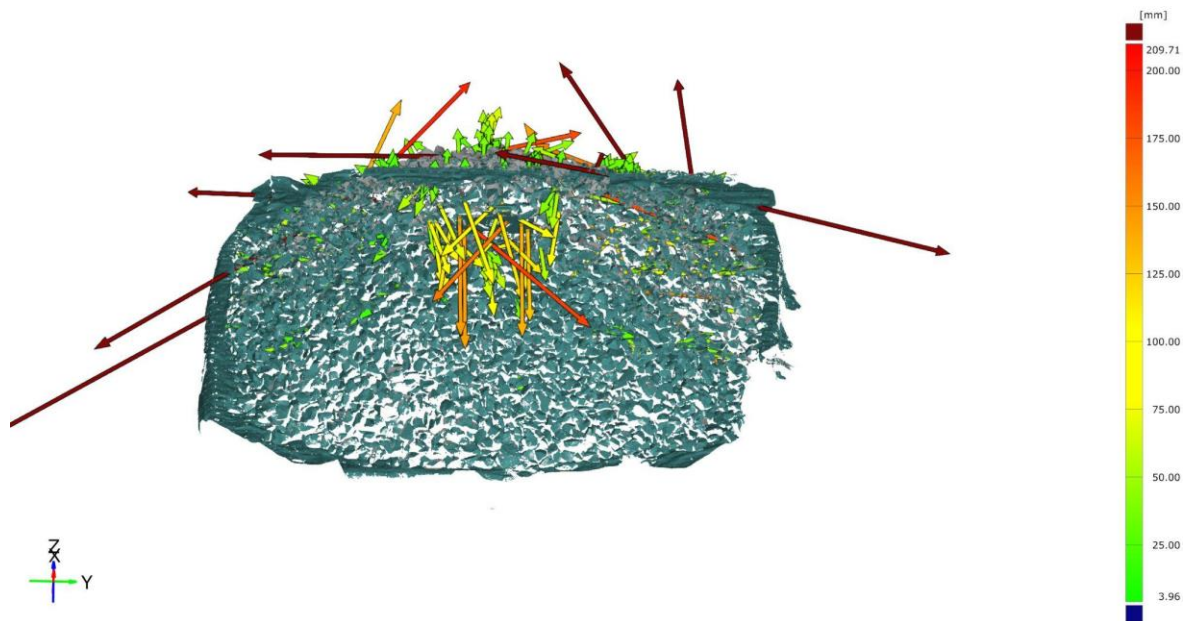
Figure 19. Displacement of the test sample in 3D, axonometric view – GOM TRITOP #2 (the long brown and red arrows can be neglected, they are related to the enconded reference points)
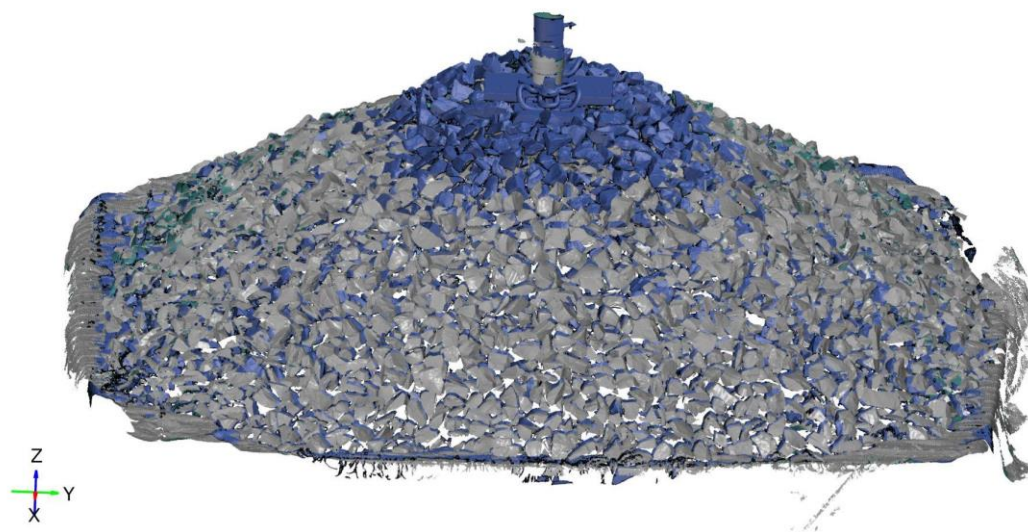
Figure 20. Displacement of the test sample in 3D, axonometric view – GOM ATOS #2 (the blue elements are the CAD model, i.e., the original state or in other words: the state before the loading; the gray elements are the are the mesh model, i.e., the state with displacement or in other words: the state after the loading)
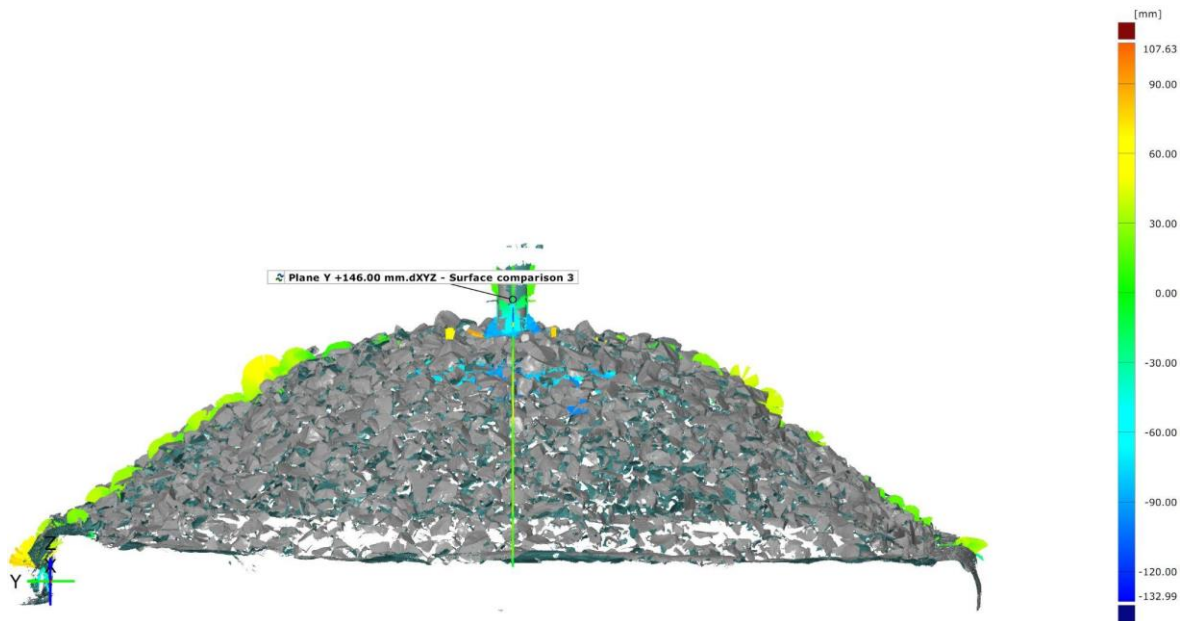
Figure 21. Displacement of the test sample in 3D, combined cross-section and axonometric view – GOM ATOS #2

These significant deformations are confirmed by the displacement curves and trajectories made by GOM software. The cross-sectional diagrams show the change between the initial and final states (Figs. 22-25).
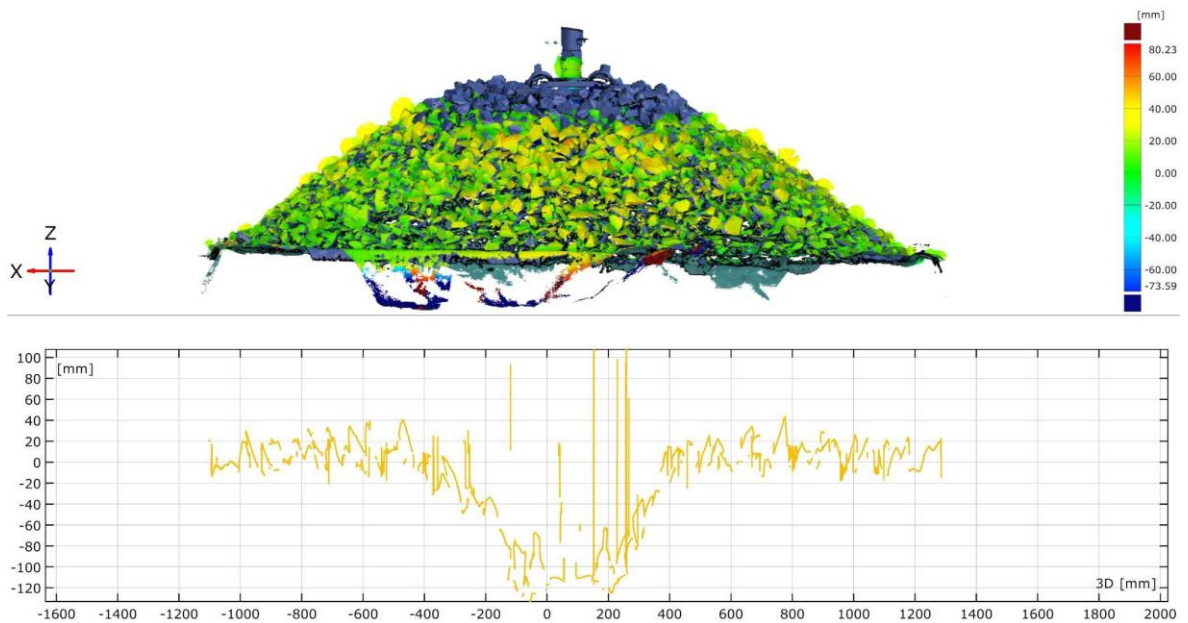
Figure 22. Displacement of the test sample in 3D, cross-section – GOM ATOS #1
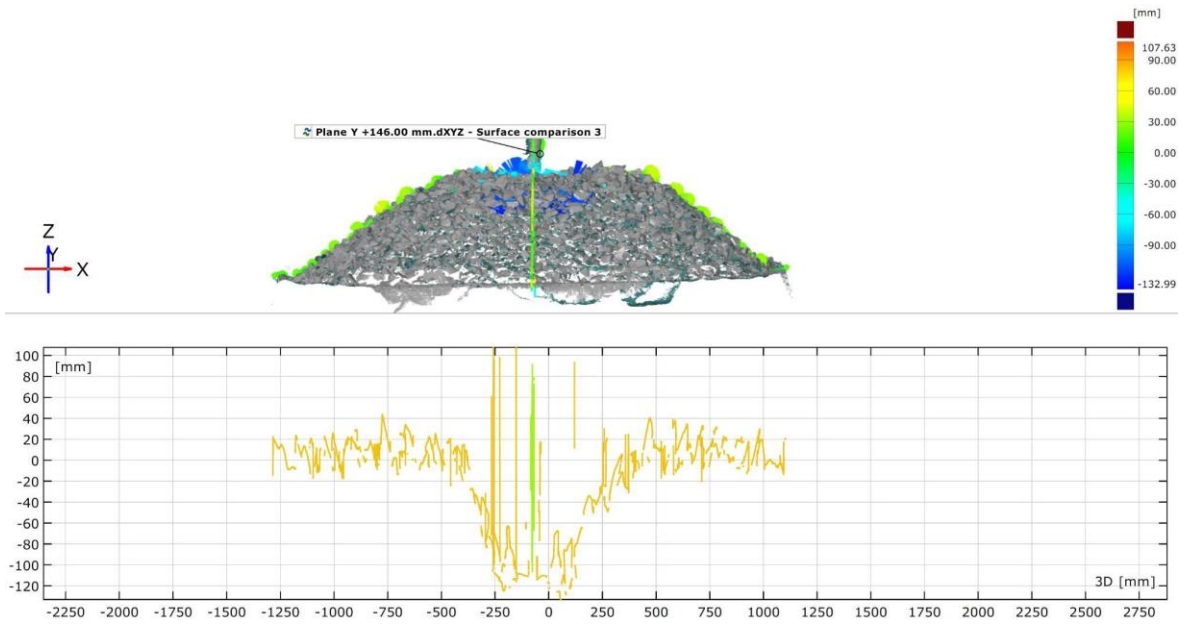
Figure 23. Displacement of the test sample in 3D, cross-section – GOM ATOS #2
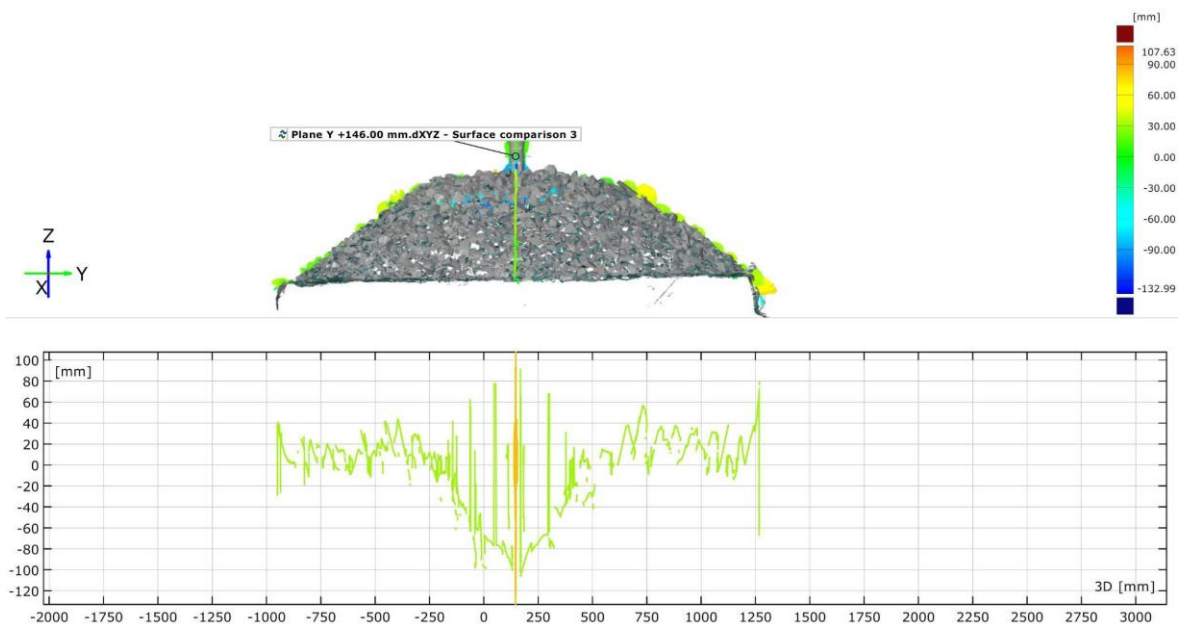
Figure 24. Displacement of the test sample in 3D, cross-section – GOM ATOS #3
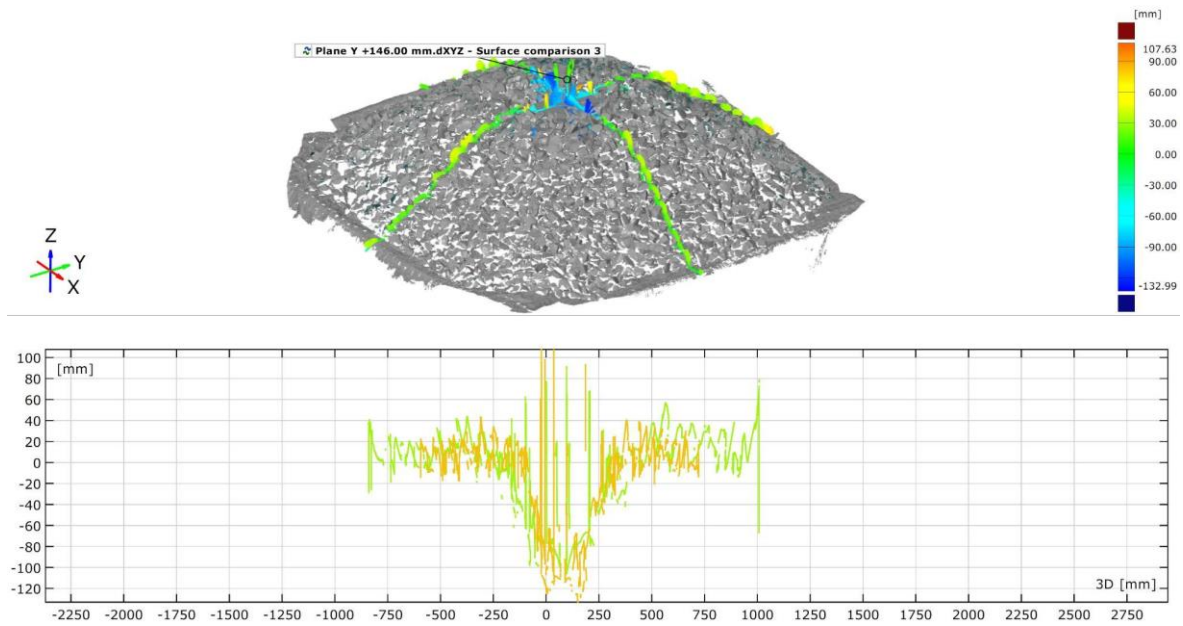
Figure 25. Displacement of the test sample in 3D, the position of the cross-section planes – GOM ATOS

The authors have chosen two pieces of dedicated colored crushed stones on them, so they can show the particle breakage (fragmentation). These two particles were the *Orange #1* and the *Blue #1* stones. Blue #1 stone is represented in Figs. 26-30, while the *Orange #1* is in Figs. 31-35. The first one (*Blue #1*) was directly under the sleeper's bottom, while the second one (*Orange #1*) was 15 cm below the sleeper. The abrasion is visible to the eye (on the colored ones), but thanks to the DICM investigations, the 3D scanned stones showed the wear with an accuracy of 0.1 mm (Figs. 28-30 and Figs. 33-35). In these figures, on the bottom left corner, the arrows represent the coordinate system to see the side of the viewpoints.

Figure 26. *Blue #1* stone in the fragmented, broken ballast (i.e., after the loading test)

Figure 27. *Blue #1* stone after the experiment
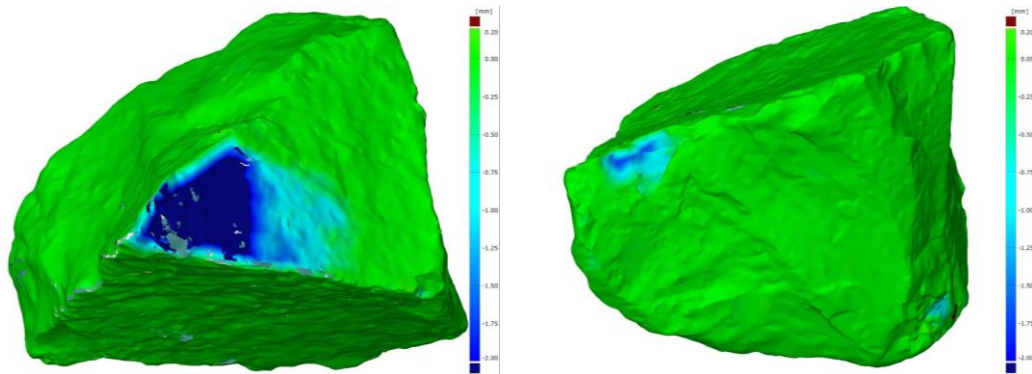
Figure 28. Scanned *Blue #1* stone after the experiment
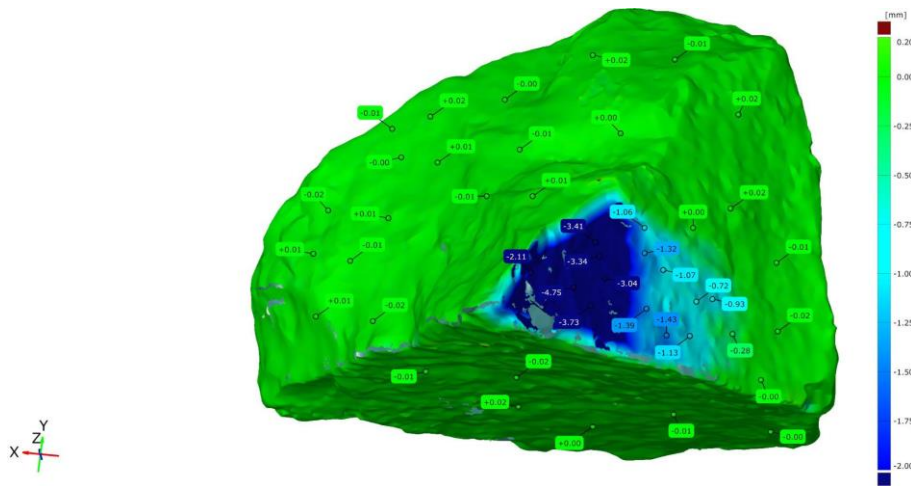
Figure 29. Scanned *Blue #1* stone after the experiment – deformation with flags indicated #1
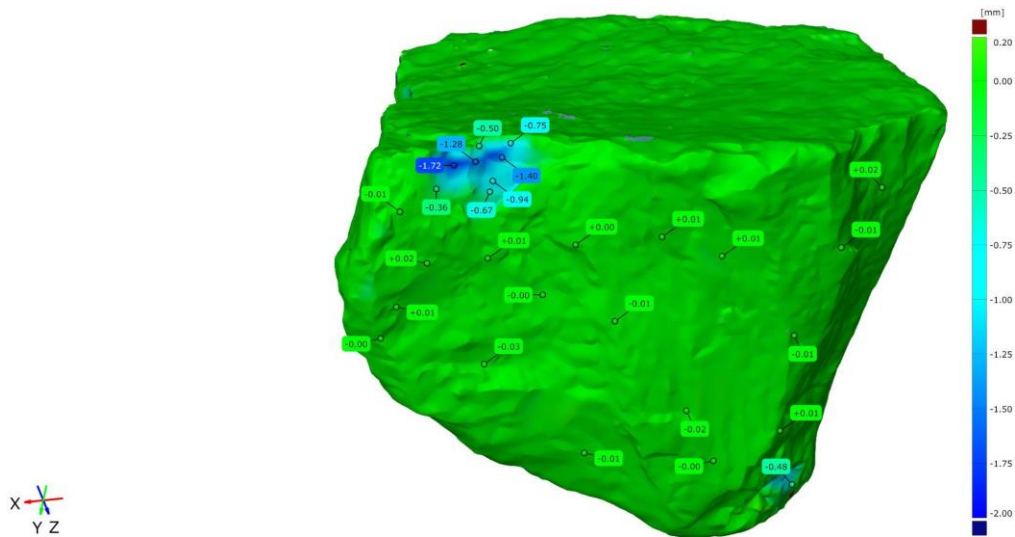
Figure 30. Scanned *Blue #1* stone after the experiment – deformation with flags indicated #2

Figure 31. *Orange #1* stone in the fragmented, broken ballast

Figure 32. *Orange #1* stone after the experiment
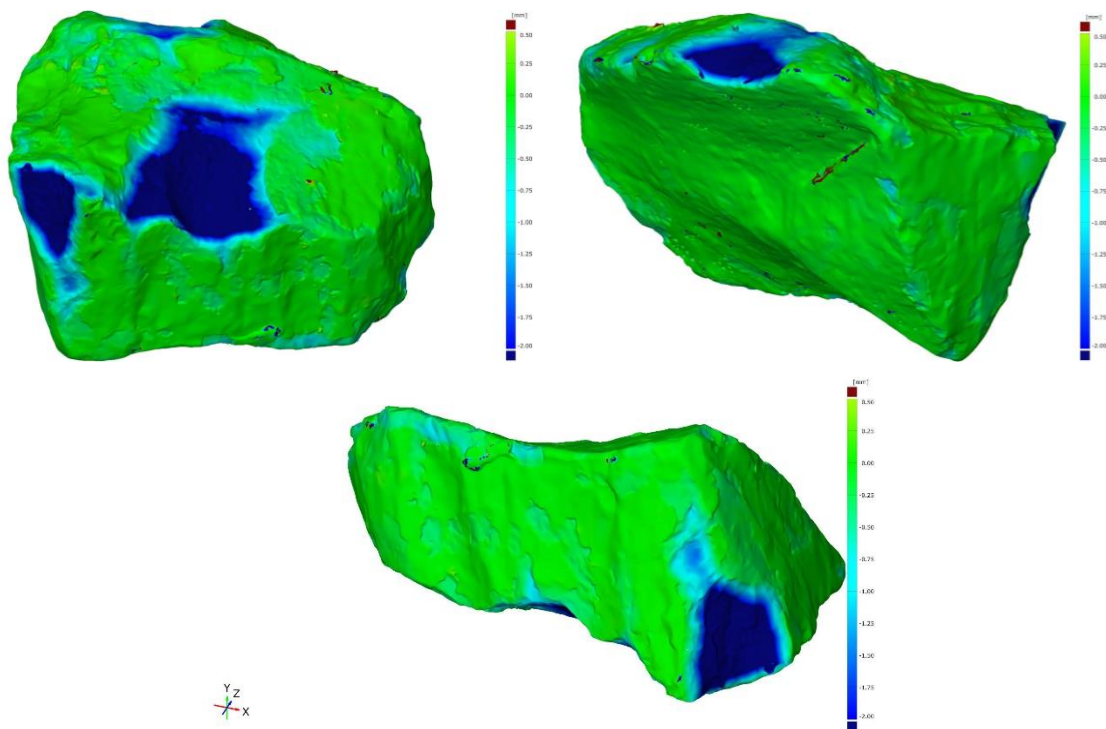
Figure 33. Scanned *Orange #1* stone after the investigation
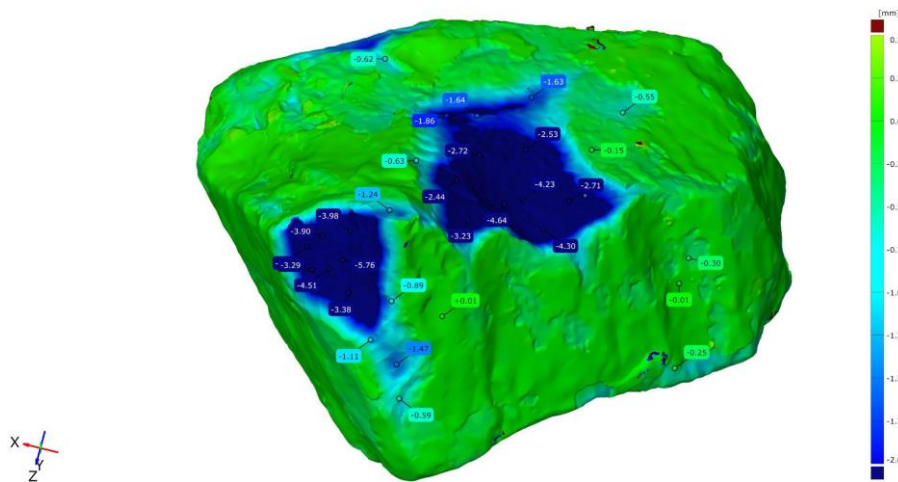
Figure 34. Scanned *Orange #1* stone after the experiment – deformation with flags indicated #1
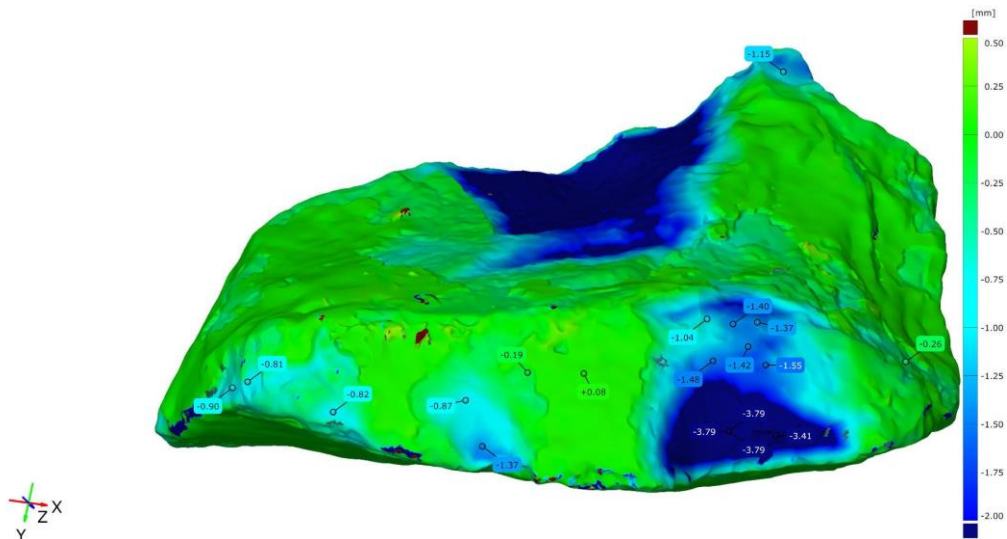
Figure 35. Scanned *Orange #1* stone after the experiment – deformation with flags indicated #2

It can be seen in the scanned figures (Figs. 28-30 and Figs. 33-35) that the significant abrasion and breakage was at the edges of the stones, while the surface was not worn significantly. The reason for that is the static loading. It is clear that this measurement could be an excellent and spectacular method for investigating abrasion.

The DICM measurement can scan the outer structure (surface) of the sample, which is very important to define the settlements (i.e., displacement and deformation). Therefore the authors also registered the coordinates of the stone in a local x-y-z Descartes coordinate system during the set-up (i.e., before loading) and during the disassembling (i.e., after loading). The [0;0;0] reference point was the upper corner of the OSB frame. In addition, the center of the load is [100;110;z], where the z was 58 cm (i.e., 35+23 cm, where 35 is the thickness of the ballast bed and 23 is the height of the sleeper), but the loading was distributed on the lower plane of the 29×39 cm size concrete sleeper. The stones' original locations and their place after the loading can be seen in the following table. The authors determined the displacement in vector form from the coordinates, in [cm] dimension.

Table 2. The displacement of the registered stone particles

Registered stone	Original place (position) [cm]	Place (position) after loading [cm]	Displacement [cm]
Blue #1	100;110;35	105;111;20	5;1;-15
Orange #1	119;109;20	125;103;10	6;-6;-10

During the disassembly of the aggregate, it was visually perceptible (it was clearly visible) that the greatest fragmentation occurred in the layers below the loaded zone. Upon removing the layers, more and more dust and broken stone particles were observed (Fig. 36).

Prior to the research, similar results were able to be observed on smaller sets (Juhász & Fischer, 2019b).

The 3D measurement method, despite the difficulties, is unequivocally suitable for measuring the displacements of the railway crushed stone bedding (as small granular materials) and, consequently, in conclusion, where the greatest deformations occurred, there were also the greatest stresses within the ballast bed.

Figure 36. Dust and broken stone particles found in the lower layers

Despite the spectacular results, the authors had to realize that the test design is needed to improve for the following reasons:

- the bending stiffness of the frame of OSB sheets,
- due to the large deformation of the sandy gravel layer (unfortunately, the authors were not able to provide the appropriate $E_{2,stat}$ load-bearing capacity during the laboratory conditions),
- due to the time required for 3D scanning,
- the authors plan to reduce the test forces (by the actuator) to values close to reality (e.g., application of a reduced value calculated for the contact surface of the applied quarter-size reinforced concrete sleeper),
- different layer orders are planned for use (e.g., application of under sleeper pads and concrete canvas)

5. Conclusions and future research possibilities

The authors certified – based on their laboratory experiment and related investigation – that the GOM 3D measurement methods (GOM ATOS and GOM TRITOP), despite the happened and arisen difficulties, is unequivocally suitable for measuring the displacements and deformations of the railway ballast bed (as relatively small granular materials in high quantity which formulate high "test sample").

If the test is constructed with a modified layer order (set-up), the authors' goal is to repeat this measurement in order to get a more accurate, spectacular test image. The test can be executed with static and dynamic loading, as well.

From the aspect of the railways, the DICM measurement provides a new, more accurate method to determine the settlements and the degree of abrasion. For example, scanning the selected colored stones can show us the wearing with an accuracy of 0.01 to 0.1 mm. On the other hand, the DICM can measure the surface of a rigid sample, for example, asphalt concrete layer, Concrete Canvas layer, etc. Thanks to this, it can open a new perspective of measuring the settlement of the lower layers too.

The application of DIC methods can be improved by the most modern techniques in this field, i.e., GOM ARAMIS, GOM ARAMIS SRX, recording of deformations with the help of video with up to 600 Hz frequency, etc.

References

Ahmad, M. (2021). Review of materials used for ballast reinforcement. Acta Technica Jaurinensis, 14(3), 315–338. https://doi.org/10.14513/actatechjaur.00610.

Buń, P., Górski, F., Wichniarek, R., Kuczko, W., Hamrol, A., & Zawadzki, P. (2015). Application of Low-cost Tracking Systems in Educational Training Applications. Procedia Computer Science, 75, 398–407. https://doi.org/10.1016/J.PROCS.2015.12.263.

CEN (2002). EN 13450:2002: Aggregates for railway ballast. Harmonized European Union Standard.

Eller, B., Majid, M. R., & Fischer, S. (2022). Laboratory Tests and FE Modeling of the Concrete Canvas, for Infrastructure Applications. Acta Polytechnica Hungarica, 19(3), 9–20. https://doi.org/10.12700/APH.19.3.2022.3.2.

Fischer, S. (2015). Investigation of inner shear resistance of geogrids built under granular protection layers and railway ballast. Science and Transport Progress. Bulletin of Dnipropetrovsk National University of Railway Transport, 5(59), 97–106. https://doi.org/10.15802/stp2015/53169.

Fischer, S. (2017). Breakage test of railway ballast materials with new laboratory method. Periodica Polytechnica Civil Engineering, 61(4), 794–802. https://doi.org/10.3311/PPci.8549.

Fischer, S. (2021). Investigation of effect of water content on railway granular supplementary layers. Scientific Bulletin of National Mining University, 2021(3), 64–68. https://doi.org/10.33271/nvngu/2021-3/064.

Fischer, S. (2022). Investigation of the Horizontal Track Geometry regarding Geogrid Reinforcement under Ballast. Acta Polytechnica Hungarica, 19(3), 89–101. https://doi.org/10.12700/APH.19.3.2022.3.8.

Funke, C. (2016). GOM 3D Metrology Systems. https://www.k3works.de/fileadmin/user_upload/News/005_presentation_optical_measurement.pdf (Accessed: 16 January 2022).

Goda, I., Lhostis, G., & Guerlain, P. (2019). In-situ non-contact 3D optical deformation measurement of large capacity composite tank based on close-range photogrammetry. Optics and Lasers in Engineering, 119, 37–55. https://doi.org/10.1016/j.optlaseng.2019.02.006.

GOM (2022). GOM Metrology to Go. https://www.gom.com/en/explore-gom/gom-metrology-to-go (Accessed: 5 January 2022).

GOM GmbH (2011). GOM ATOS III Triple Scan User Manual. https://www.manualslib.com/products/Gom-Atos-Iii-Triple-Scan-10970231.html (Accessed: 10 January 2022).

Grossoni, I., Powrie, W., Zervos, A., Bezin, Y., & Le Pen, L. (2021). Modelling railway ballasted track settlement in vehicle-track interaction analysis. Transportation Geotechnics, 26, 100433. https://doi.org/10.1016/j.trgeo.2020.100433.

Guochong, L., & Haiyan, Y. (2021). Preparation and Mechanical Properties of Polyurethane Material for Railway Ballast. Science of Advanced Materials, 13(7), 1238–1245. https://doi.org/10.1166/sam.2021.4007.

Habashneh, M. (2021). Special reinforcement solutions of railway permanent ways' soil substructures. Acta Technica Jaurinensis, 14(3), 339–363. https://doi.org/10.14513/actatechjaur.00612.

Hungarian Standards (1989). MSZ 2509-3:1989: Static load plate test

Hungarian State Railways (2020). e-VASUT 02.10.20 D.11: Vasúti alépítmény tervezése, építése, karbantartása és felújítása. Retrieved from https://www.mosz.co.hu/images/a1644/MAV2004.pdf.

Jóvér, V., Gáspár, L., & Fischer, S. (2022). Investigation of Tramway Line No. 1, in Budapest, Based on Dynamic Measurements. Acta Polytechnica Hungarica, 19(3), 65–76. https://doi.org/10.12700/APH.19.3.2022.3.6.

Juhasz, E., & Fischer, S. (2019a). Specific evaluation methodology of railway ballast particles' degradation. Science and Transport Progress. Bulletin of Dnipropetrovsk National University of Railway Transport, 3(81), 96–109. https://doi.org/10.15802/stp2019/171778.

Juhász, E., & Fischer, S. (2019b). Railroad Ballast Particle Breakage with Unique Laboratory Test Method. Acta Technica Jaurinensis, 12(1), pp. 26–54. https://doi.org/10.14513/actatechjaur.v12.n1.489.

Juhász, E., & Fischer, S. (2020). Investigation of particle degradation of railway ballast materials due to static and dynamic loadings. X. International Conference on Transport Sciences, Győr, 2020, ISBN: 978963121882 547–553. https://www.researchgate.net/publication/339366240_Investigation_of_particle_degradation_of_railway_ballast_materials_due_to_static_and_dynamic_loadings (Accessed: 16 January 2022).

Juhász, E., & Fischer, S. (2021). Tutorial on the fragmentation of the railway ballast particles and calibration methods in discrete element modelling. Acta Technica Jaurinensis, 14(1), 104-122. https://doi.org/10.14513/actatechjaur.00569.

Koutecký, T., Paloušek, D., & Brandejs, J. (2013). Method of photogrammetric measurement automation using TRITOP system and industrial robot. Optik - International Journal for Light and Electron Optics, 124(18), 3705–3709. https://doi.org/10.1016/J.IJLEO.2012.11.024.

Kurhan, D., & Kurhan, M. (2019). Modeling the dynamic response of railway track. In IOP Conference Series: Materials Science and Engineering (IOP Publishing), 708(1), 012013. https://doi.org/10.1088/1757-899X/708/1/012013.

Kurhan, D., & Havrylov, M. (2020). The Mathematical Support of Machine Surfacing for the Railway Track. Acta Technica Jaurinensis, 13(3), 246-267. https://doi.org/10.14513/actatechjaur.v13.n3.556.

Kurhan, D., & Leibuk, Y. (2020). Research of the Reduced Mass of the Railway Track. Acta Technica Jaurinensis, 13(4), 324–341. https://doi.org/10.14513/actatechjaur.v13.n4.563.

Kurhan, D. M., & Fischer, S. (2022). Modeling of the Dynamic Rail Deflection using Elastic Wave Propagation. Journal of Applied and Computational Mechanics, 8(1), 379–387. https://doi.org/10.22055/jacm.2021.38826.3290.

MABA Hungaria Ltd. (2017). Product datasheet, L4 type concrete sleeper https://www.maba.hu/de/pog3/streckenschwellen/ (Accessed: 18 January 2022).

Przybyłowicz, M., Sysyn, M., Gerber, U., Kovalchuk, V., & Fischer, S. (2022). Comparison of the effects and efficiency of vertical and side tamping methods for ballasted railway tracks. Construction and Building Materials, 314, 125708. https://doi.org/10.1016/j.conbuildmat.2021.125708.

Rampat, Chandr Toshan (2018) Reinforcement of ballasted railway tracks using 3D-geocomposite. MPhil thesis, University of Nottingham. http://eprints.nottingham.ac.uk/51991/ (Accessed: 16 January 2022).

R-Design Studio (2022). TRITOP http://r-design.hu/merorendszerek-szoftverek/tritop/ (Accessed: 16 January 2022).

Sysyn, M., Nabochenko, O., Gerber, U. & Kovalchuk, V. (2019). Evaluation of railway ballast layer consolidation after maintenance works. Acta Polytechnica, 58 (6), 1–16.

Sysyn, M., Gerber, U., Kovalchuk, V. & Nabochenko, O. (2018). The complex phenomenological model for prediction of inhomogeneous deformations of railway ballast layer after tamping works. Archives of Transport, 46 (3), 91–107, DOI: https://doi.org/10.5604/01.3001.0012.6512.

Szalai, S. (2021). Investigation of formability of aluminum vehicle body sheets. Ph.D. thesis, Széchenyi István University (in Hungarian). https://doktori.hu/index.php?menuid=193&lang=HU&vid=23285 (Accessed: 16 January 2022).

Szalai, S., & Dogossy, G. (2021). Speckle pattern optimization for DIC technologies. Acta Technica Jaurinensis, 14(3), 228–243. https://doi.org/10.14513/actatechjaur.00573.

Szalai, S., Szürke, S. K., Harangozó, D., & Fischer, S. (2022). Investigation of deformations of a lithium polymer cell using the Digital Image Correlation Method (DICM). Reports in Mechanical Engineering, 3(1), 206–224. https://doi.org/10.31181/rme20008022022s.

Transcalc (2022). CALCULATION AND PLOTTING TOOLS. Sieve Analysis Calculation and Plotting http://www.transcalc.com/sieveanalysiscalc (Accessed: 10 January 2022).